Electronic Supplementary Information

A novel red-emitting phosphor $K_2MgGeO_4:Eu^{3+}$ for WLED: zero-thermal quenching induced by heterovalent substitution

Yuxing Bai,[a] Zhenwei Jia,[a] Jingyi Gao,[a] Li Wu,[a,] Yongfa Kong,*[a] Yi Zhang,[b] and Jingjun Xu [a]

[a]Key Laboratory of Weak-Light Nonlinear Photonics, Ministry of Education, School of Physics, Nankai University, Tianjin 300071, China. E-mail: *lwu@nankai.edu.cn
[b]Institute of Photo-electronic Thin Film Devices and Technology, Nankai University, Tianjin 300071, China

Experimental section

Materials and synthesis: The samples $K_{2-x}MgGeO_4:xEu^{3+}$ ($0.02 \leq x \leq 0.14$) were synthesized via a high-temperature solid-state method in an ambient atmosphere. The original raw materials were K_2CO_3 (99.99%), MgO (99.99%), GeO_2 (99.99%), and Eu_2O_3 (99.99%). All of them were weighted according to the molar ratio and thoroughly mixed in an agate mortar. Then the processed mixtures were pre-heated at 600 °C for 12 h in a crucible to decompose the carbonates and eliminate water. After cooling to room temperature, the pre-sintered samples were reground and sintered at 1100 °C for 24 h. Finally, the sintered products were well ground into powders to use in subsequent performance characterizations.

Characterization: Powder XRD patterns were collected on a D8 ADVANCE diffractometer (X'Pert Pro, PANalytical B.V., Netherlands) operating at 40 kV and 40 mA with Cu Kα radiation (λ = 1.5406 Å). The refinement data for Rietveld analysis were gathered in step-scanning mode over the 2θ range from 10° to 130° at intervals of 0.017°. The photoluminescence (PL) and photoluminescence excitation (PLE) spectra at room temperature were measured using a fluorescence spectrometer (Edinburgh Instruments, FLS920, England) equipped with a 150 W Xenon lamp. The photoluminescence quantum yield (PLQY) was measured using a calibrated integrating sphere. The fluorescence lifetime of millisecond was obtained using a 100 w μF900 lamp as the light source and a R928P photo-multiplier as the detector. The temperature-dependent luminescence properties were also studied using the same spectrofluorometer with a heating apparatus (Tianjin Orient Koji Co., Ltd, TAP-02). Scanning electron microscopy (SEM, SU8020, HITACHI, Japan) with energy dispersive X-ray spectroscopy (EDX, EMAX, HORIBA) was used to characterize the morphology of the samples. X-ray photoelectron spectroscopy (XPS) were recorded using a Thermo Scientific ESCALAB 250Xi (America) and calibrated to a C 1*s* electron peak at 284.8 eV. Inductively Coupled Plasma-Optical Emission Spectrometer (ICP-OES) was considered to examine the amounts of all the elements by means of Agilent ICPOES730 (America) with the power of 1.0 KW. After pre-irradiating with 365 nm UV light for 15 min, thermoluminescence (TL) curves of the powder samples were obtained using a thermoluminescence meter (FJ427A1, CNCS, China). The CIE coordinate (x, y) was calculated from the emission spectra through the CIE calculator. Based on that, the CCT (K) values were approximated by the following equation:[1]

$$CCT = -437 \times n^3 + 3601 \times n^2 - 6861 \times n + 5541.31 \quad (1)$$

where n is $(x\text{-}x_c)/(y\text{-}y_c)$ and (x_c = 0.3320, y_c = 0.1858) is the chromaticity epicenter. The color purity can be calculated via using the obtained CIE coordinates, as expressed by the following equation:[2]

$$Color\ purity\ (\%) = \frac{\sqrt{(x_s - x_i)^2 + (y_s - y_i)^2}}{\sqrt{(x_d - x_i)^2 + (y_d - y_i)^2}} \quad (2)$$

where (x_s, y_s), (x_d, y_d), and (x_i = 0.33, y_i = 0.33) are the CIE coordinates of the as-prepared phosphors, the dominant

wavelength, and the reference white illuminant point, respectively.

Computational methods: All the DFT calculations were implemented with the Vienna ab initio simulation package (VASP). The electron-ion interactions were determined using the projector augmented wave pseudo-potential method.[3] Periodic DFT calculations were performed using the PBE+U approach with U = 2.5 eV for the Eu 4f electrons. K ($4s^1$), Mg ($3s^2$), Ge ($3d^{10}4s^24p^2$), O ($2s^22p^4$), and Eu ($5s^25p^64f^76s^2$) electrons were treated as their own valence electrons. To investigate the density of states accurately, the spin-polarized generalized gradient approximation with the Perdew-Burke-Ernzerhof functional was adopted to describe the electronic exchange-correlation potential.[4] The cutoff energy of 400 eV was used for the plane-wave basis set to expand the pseudo valence wave function. A 2 × 2 × 1 supercell was constructed, in which K^+ ions were substituted by Eu^{3+} ions. Moreover, k-point grids for the Brillouin zone were generated with 5 × 5 × 5 and 1 × 1 × 1 G-centered models for the primitive-cell and super-cell, respectively. All the optimization processes were considered to satisfy the convergence criterion when the total energy change was less than 1×10^{-4} eV per step, and the maximum force was less than 3×10^{-2} eV $Å^{-1}$ per atom.

LED fabrication: The WLED was successfully fabricated through combining commercial blue phosphor $BaMgAl_{10}O_{17}:Eu^{2+}$, green phosphor $(Sr, Ba)_2SiO_4:Eu^{2+}$ and our red phosphor $K_{1.9}MgGeO_4:0.10Eu^{3+}$ with a UV-LED chip (λ = 394 nm). The phosphors were thoroughly mixed with epoxy resin, and the obtained phosphor-epoxy resin mixture was coated on the LED chip. The photoelectric properties, including the electroluminescent (EL) spectrum, luminous efficacy, CCT, color rendering index (R_a) as well as CIE color coordinates of the LED were characterized by using a photometry colorimeter & electricity test system equipped with an integrating sphere (HP9000, Hopoo, China).

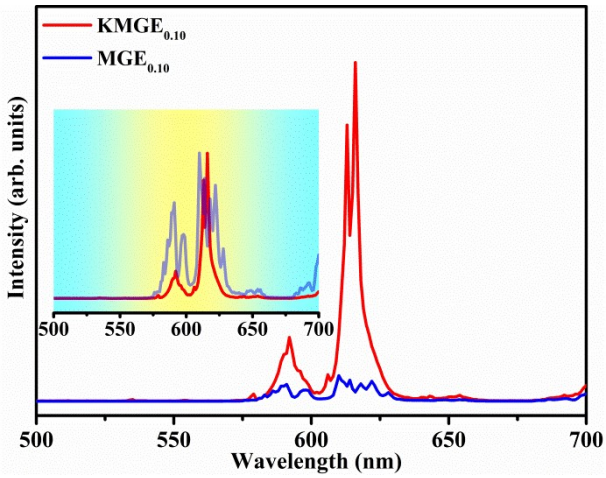

Fig. S1 PL spectra of $K_{1.9}MgGeO_4:0.10Eu^{3+}$ and $MgGeO_3:0.10Eu^{3+}$ (λ_{ex} = 394 nm, λ_{em} = 616 nm).

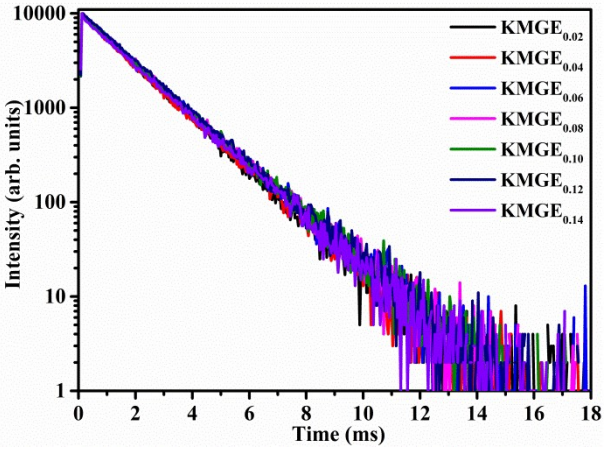

Fig. S2 Decay curves of $K_{2-x}MgGeO_4:xEu^{3+}$ ($0.02 \leq x \leq 0.14$, λ_{ex} = 394 nm, λ_{em} = 616 nm).

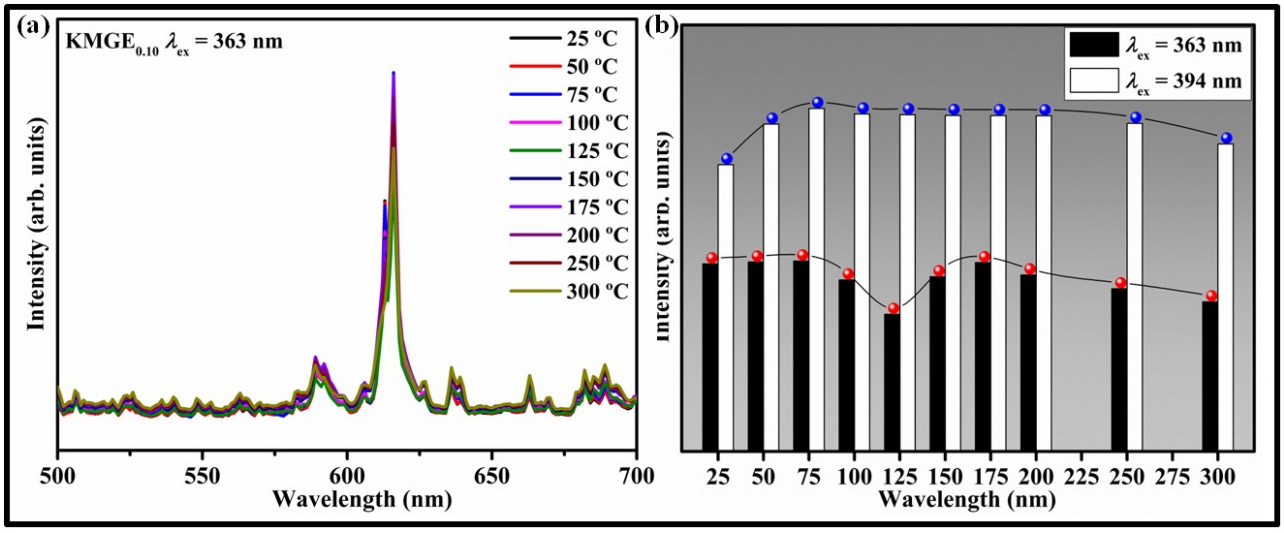

Fig. S3 (a) Temperature-dependent spectrum of $K_{1.9}MgGeO_4:0.10Eu^{3+}$ (λ_{ex} = 363 nm, λ_{em} = 616 nm). (b) The relationship between temperature and emission intensity (λ_{ex} = 363 nm, 394 nm; λ_{em} = 616 nm).

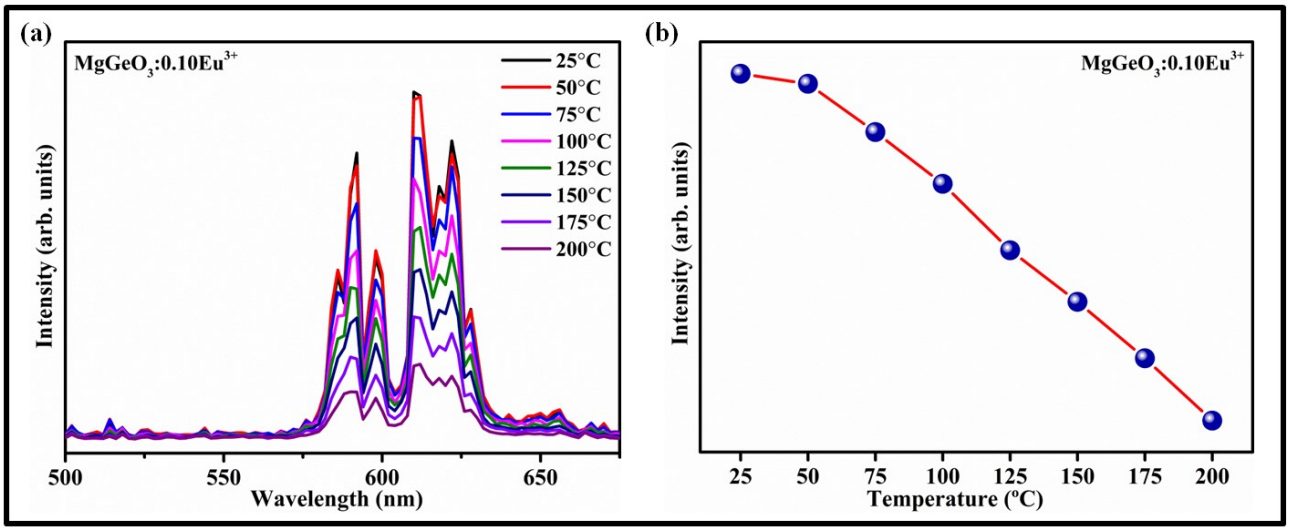

Fig. S4 (a) Temperature-dependent spectrum of $MgGeO_3:0.10Eu^{3+}$ (λ_{ex} = 394 nm, λ_{em} = 616 nm). (b) The relationship between temperature and emission intensity (λ_{ex} = 394 nm, λ_{em} = 616 nm).

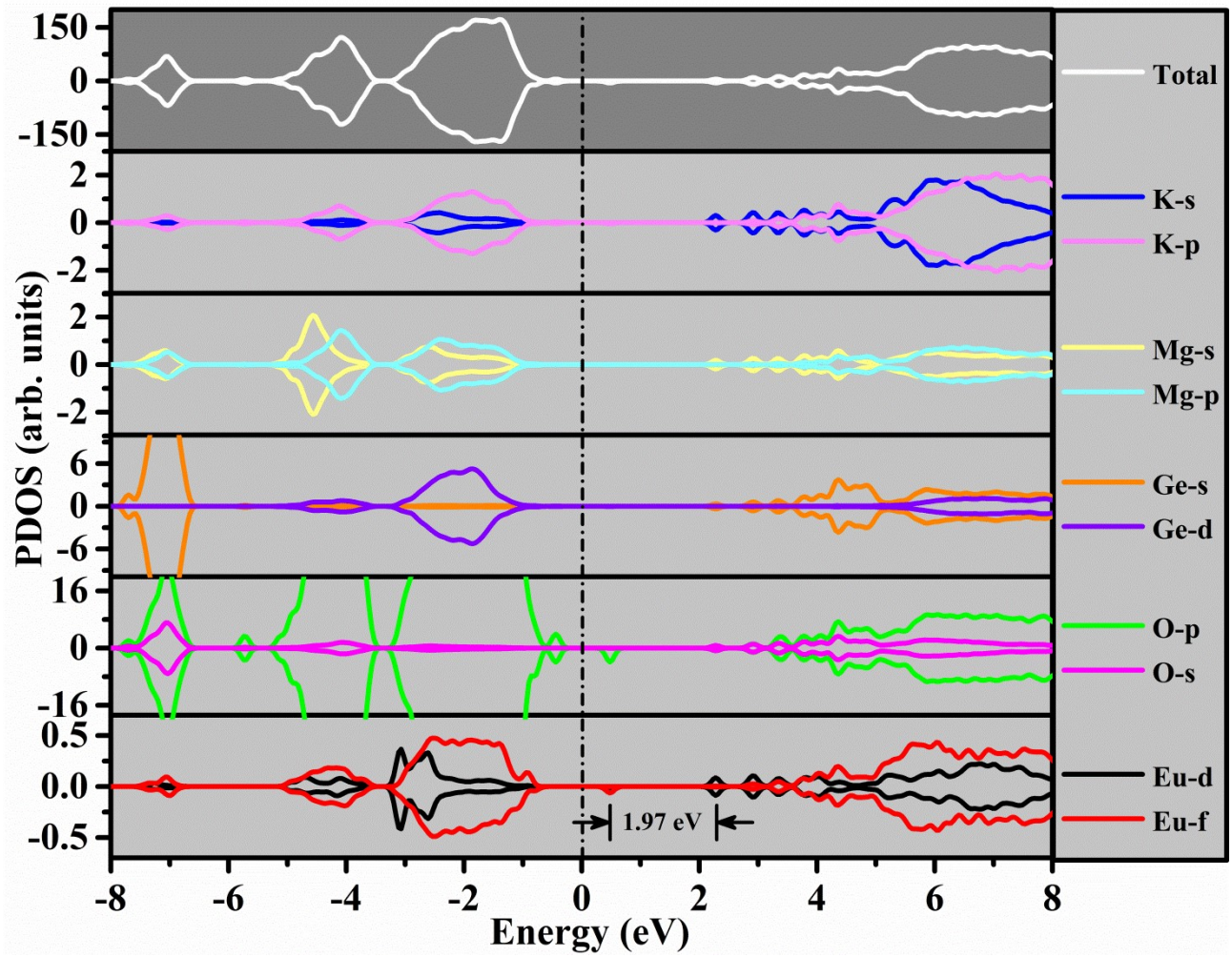

Fig. S5 Total and partial density of states for $K_{1.9}MgGeO_4$:0.10Eu^{3+}.

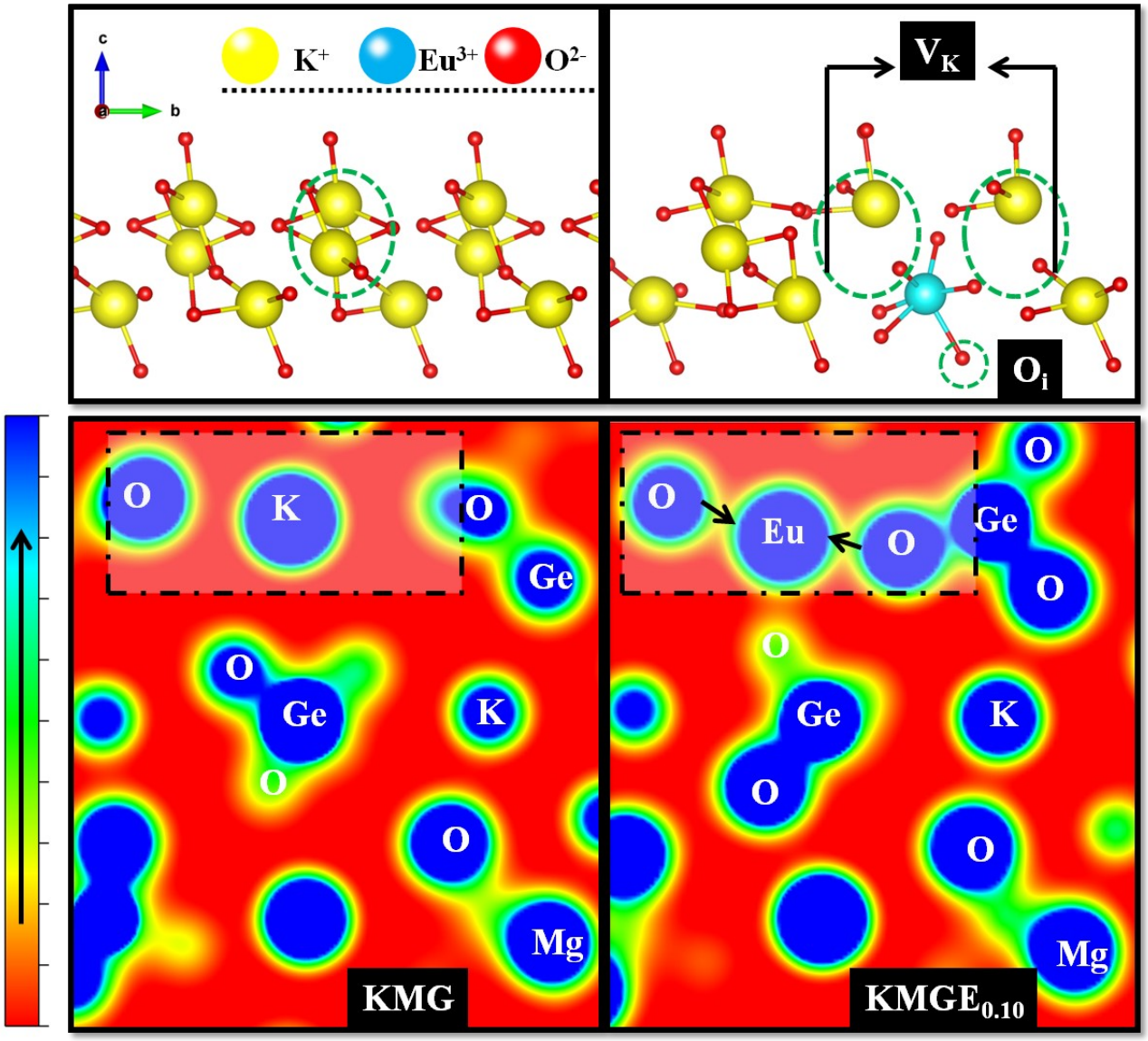

Fig. S6 Local coordinated structures and two-dimensional electron localization function (ELF) maps around K/Eu sites for K_2MgGeO_4 and $K_{1.9}MgGeO_4$:0.10Eu^{3+}+V_K+O_i.

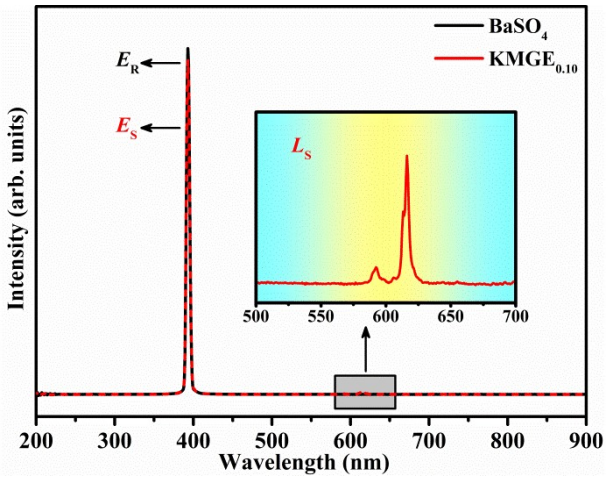

Fig. S7 The excitation line of $BaSO_4$ and the emission spectrum of the $K_{1.9}MgGeO_4$:0.10Eu^{3+} phosphors collected using an integrating sphere. The inset shows a magnification of the emission spectrum.

As shown in Fig. S6, the internal quantum efficiency (IQE) value can be calculated by the following equation:[5]

$$\eta_{QE} = \frac{\int L_S}{\int E_R - \int E_S} \tag{3}$$

where E_R is the spectrum of the excitation light without the sample in the sphere, E_S is the spectrum of the light used for exciting the sample, and L_S is the emission spectrum of the targeted sample.

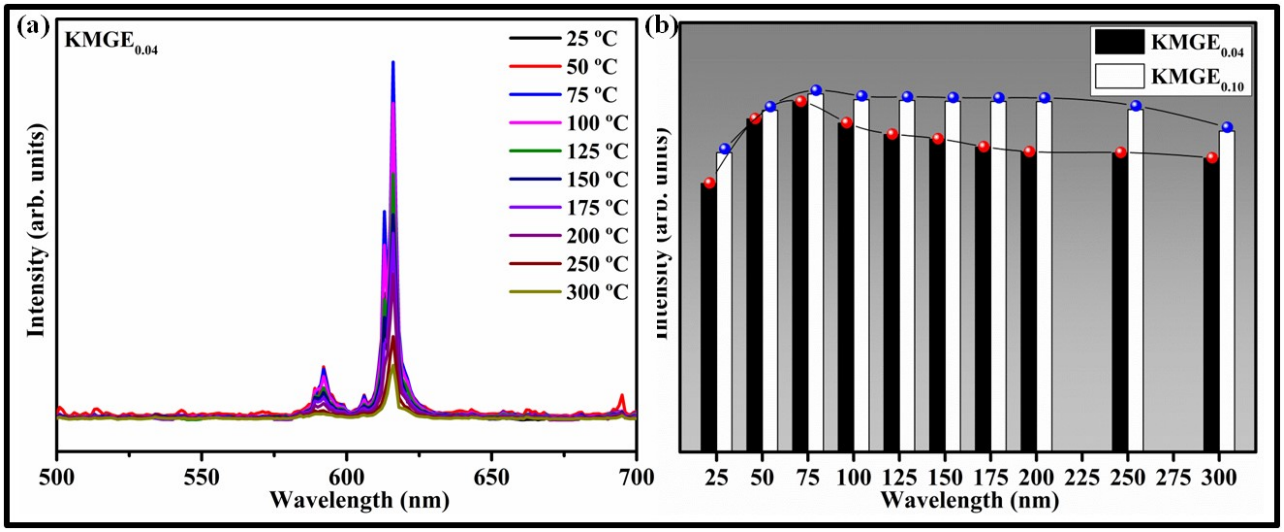

Fig. S8 (a) Temperature-dependent spectrum of $K_{1.96}MgGeO_4$:0.04Eu^{3+} (λ_{ex} = 394 nm, λ_{em} = 616 nm). (b) The relationship between temperature and emission intensity of $K_{1.96}MgGeO_4$:0.04Eu^{3+} and $K_{1.9}MgGeO_4$:0.10Eu^{3+} (λ_{ex} = 394 nm, λ_{em} = 616 nm).

Table S1 Lattice parameters and agreement factors for K_2MgGeO_4:0.01Eu^{3+} refined by Rietveld method when Eu^{3+} ions occupy all of the cationic sites.

Crystal system	orthorhombic
Space group	*Pca*2$_1$ (29)
a (Å)	11.1886 (3)
b (Å)	5.5724 (11)
c (Å)	15.8387 (3)
Volume (Å^3)	987.50 (4)
Z	8
R_p (%)	10.04
R_{wp} (%)	14.86
R_{exp} (%)	8.32
GOF	1.79

Table S2 Atomic positions and occupancies for K_2MgGeO_4:0.01Eu^{3+} refined by Rietveld method when Eu^{3+} ions occupy all of the cationic sites.

Np	*x*	*y*	*z*	Occupancy

K1	4	0.0047 (3)	-0.0097 (3)	0.7824 (8)	1.059 (5)
Eu1	4	0.0047 (3)	-0.0097 (3)	0.7824 (8)	-0.059 (5)
K2	4	0.0115 (2)	0.5327 (3)	0.4013 (5)	1.057 (6)
Eu2	4	0.0115 (2)	0.5327 (3)	0.4013 (5)	-0.057 (6)
K3	4	0.2261 (2)	0.0404 (3)	0.1566 (9)	1.056 (5)
Eu3	4	0.2261 (2)	0.0404 (3)	0.1566 (9)	-0.056 (5)
K4	4	0.2446 (9)	0.5632 (2)	0.9927 (8)	0.9919 (2)
Eu4	4	0.2446 (9)	0.5632 (2)	0.9927 (8)	0.0081 (2)
Mg1	4	0.0099 (3)	-0.0267 (6)	0.5258 (9)	1.083 (7)
Eu5	4	0.0099 (3)	-0.0267 (6)	0.5258 (9)	-0.083 (7)
Mg2	4	0.2397 (3)	0.5179 (3)	0.2740 (2)	1.0 (4)
Eu6	4	0.2397 (3)	0.5179 (3)	0.2740 (2)	0.0 (4)
Ge1	4	0.0057 (9)	0.4924 (12)	0.6434 (5)	1.032 (4)
Eu7	4	0.0057 (9)	0.4924 (12)	0.6434 (5)	-0.032 (4)
Ge2	4	0.2339 (11)	0.0339 (5)	0.8967 (8)	1.001 (4)
Eu8	4	0.2339 (11)	0.0339 (5)	0.8967 (8)	-0.001 (4)
O1	4	-0.0070 (3)	0.9328 (6)	0.0520 (2)	1.0
O2	4	0.0325 (3)	0.3362 (6)	0.0415 (8)	1.0
O3	4	0.0873 (3)	0.3989 (7)	0.2063 (9)	1.0
O4	4	0.1180 (4)	0.8781 (9)	0.9212 (9)	1.0
O5	4	0.1539 (5)	0.5660 (9)	0.6631 (7)	1.0
O6	4	0.1522 (3)	0.1098 (6)	0.4688 (3)	1.0
O7	4	0.2099 (2)	0.2901 (6)	0.8371 (8)	1.0
O8	4	0.2053 (3)	0.8413 (6)	0.3151 (5)	1.0

Table S3 Lattice parameters and agreement factors for $K_{1.99}MgGeO_4$:0.01Eu^{3+} refined by Rietveld method when Eu^{3+} ions occupy the K(4) site.

Crystal system	orthorhombic
Space group	*Pca*2$_1$ (29)
a (Å)	11.1883 (3)
b (Å)	5.5729 (2)
c (Å)	15.8434 (4)
Volume (Å^3)	987.86 (5)
Z	8
R_p (%)	9.94
R_{wp} (%)	14.76
R_{exp} (%)	8.32
GOF	1.77

Table S4 Atomic positions and occupancies for $K_{1.99}MgGeO_4$:0.01Eu^{3+} refined by Rietveld method when Eu^{3+} ions occupy the K(4) site.

	Np	*x*	*y*	*z*	Occupancy
K1	4	0.0081 (2)	0.0105 (3)	0.7547 (7)	0.8953 (4)
K2	4	0.0110 (9)	0.4866 (3)	0.3760 (9)	0.9335 (3)
K3	4	0.2364 (2)	0.0316 (3)	0.1299 (9)	0.9449 (3)
K4	4	0.2409 (9)	0.5524 (2)	0.9924 (8)	0.9902 (6)
Eu	4	0.2409 (9)	0.5524 (2)	0.9924 (8)	0.0098 (6)
Mg1	4	0.0105 (2)	0.0070 (4)	0.5031 (2)	1.0
Mg2	4	0.2476 (3)	0.5308 (3)	0.2809 (2)	1.0
Ge1	4	0.0073 (11)	0.5101 (9)	0.6206 (4)	1.0
Ge2	4	0.2354 (8)	0.0288 (12)	0.8753 (5)	1.0
O1	4	0.0096 (3)	0.7994 (6)	0.0912 (2)	1.0
O2	4	0.0429 (3)	0.3044 (6)	0.0190 (3)	1.0
O3	4	0.0909 (2)	0.3863 (5)	0.1943 (2)	1.0
O4	4	0.0763 (4)	0.9027 (9)	0.8896 (2)	1.0
O5	4	0.1602 (5)	0.6035 (8)	0.6486 (3)	1.0
O6	4	0.1670 (3)	0.0613 (6)	0.4612 (2)	1.0
O7	4	0.2117 (3)	0.2847 (7)	0.8233 (3)	1.0
O8	4	0.2078 (3)	0.8368 (5)	0.2980 (2)	1.0

Table S5 The fitted lifetimes of $K_{2-x}MgGeO_4:xEu^{3+}$ ($0.02 \le x \le 0.14$).

Doped concentrations	τ	χ^2
0.02	1.505	2.150
0.04	1.534	2.304
0.06	1.602	1.871
0.08	1.606	1.637
0.10	1.614	1.654
0.12	1.610	1.844
0.14	1.590	2.127

Table S6 The CIE chromaticity coordinates, CCT, $(^5D_0 \rightarrow {}^7F_2)/(^5D_0 \rightarrow {}^7F_1)$, and color purity of $K_{2-x}MgGeO_4:xEu^{3+}$ ($0.06 \le x \le 0.14$).

Doped concentrations (mol)	CIE coordinates (*x*, *y*)	CCK (K)	$(^5D_0 \rightarrow {}^7F_2)/(^5D_0 \rightarrow {}^7F_1)$	Color purity (%)
$x = 0.06$	(0.6641, 0.3356)	3268	6.10	99.50
$x = 0.08$	(0.6641, 0.3356)	3269	6.17	99.50
$x = 0.10$	(0.6642, 0.3355)	3272	6.21	99.53
$x = 0.12$	(0.6609, 0.3387)	3095	5.15	99.51
$x = 0.14$	(0.6606, 0.3390)	3080	5.07	99.51

Table S7 The amounts of all the elements through ICP-OES analysis for $K_{1.9}MgGeO_4:0.10Eu^{3+}$.

Sample	Wt%	Elements				
		K	Mg	Ge	O	Eu
$KMGE_{0.10}$	Theoretical	27.34	9.90	30.10	26.39	6.27
	Experimental	25.10	9.16	28.87	30.98	5.89

Table S8 The total free energies of K_2MgGeO_4 and $K_{1.9}MgGeO_4$:0.10Eu^{3+} when Eu^{3+} ions occupy different cationic sites.

Samples	KMG	$KMGE_{0.10}$					
		Eu-K1	Eu-K2	Eu-K3	Eu-K4	Eu-Mg1	Eu-Mg2
Total energy (eV)	-1411.263	-1419.332	-1419.371	-1419.351	-1419.455	-1416.833	-1416.643

Table S9 The total free energies and defect formation energies of $K_{1.9}MgGeO_4$:0.10Eu^{3+} when the lattice has different kinds of defects.

Sample	$KMGE_{0.10}$		
	Without defects	With defects	
		V_K	V_K+O_i
Total energy (eV)	-1419.455	-1403.201	-1428.195
Defect formation energy (eV)	-	5.85	-3.45

Table S10 The CCT, R_a, and CIE chromaticity coordinates under different currents (20-300 mA) for the fabricated WLED.

Current (mA)	CIE (x, y)	CCT	R_a
20	(0.3084, 0.3402)	6648	91.7
40	(0.3008, 0.3395)	7050	92.9
60	(0.3066, 0.3363)	6770	91.1
80	(0.3024, 0.3357)	7006	88.9
100	(0.3050, 0.3339)	6884	90.9
120	(0.3036, 0.3335)	6960	91.1
140	(0.3036, 0.3323)	6976	90.9
160	(0.3029, 0.3313)	7027	90.8
180	(0.3010, 0.3308)	7144	90.9
200	(0.3012, 0.3395)	7148	90.6
220	(0.3005, 0.3285)	7201	90.7
240	(0.2995, 0.3273)	7276	90.3
260	(0.2984, 0.3261)	7361	90.3
280	(0.2972, 0.3252)	7451	90.7
300	(0.2962, 0.3249)	7515	90.8

Notes and references

1 D. A. Hakeem, D. H. Kim, S. W. Kim, and K. Park, *Dyes Pigm*., 2019, **163**, 715-724.
2 Y. Li, C. D. Gong, C. G. Li, K. P. Ruan, C. Liu, H. Liu, and J. W. Gu, *J. Mater. Sci. Technol*., 2021, **82**, 250-256.
3 B. Y. Qu, B. Zhang, L. Wang, R. L. Zhou, and X. C. Zeng, *Chem. Mater*., 2015, **27**, 2195-2202.
4 J. P. Perdew, W. T. Yang, K. Burke, and A. Görling, *P. NATL. ACAD. SCI*., 2017, **114**, 2801-2806.
5 Y. J. Liu, G. X. Zhang, J. B. Huang, X. M. Tao, G. H. Li, and G. M. Cai, *Inorg. Chem*., 2021, **60**, 2279-2293.